The Lightweight Integrated Solar Array and anTenna: 3rd Generation Advancements, and Beyond

John A. Carr,[*] Les Johnson,[†] Darren Boyd,[‡] Brandon Phillips[§], and Miria Finckenor.[**]
National Aeronautics and Space Administration (NASA), Marshall Space Flight Center (MSFC), Huntsville, AL, 35812, USA

Brandon Farmer,[††] and Joseph C. Smith[‡‡]
NeXolve Corporation, Huntsville, AL, 35805, USA

This paper describes the third-generation advancements and Technology Readiness Level 6 (TRL-6) testing of NASA's Lightweight Integrated Solar Array and anTenna (LISA-T). LISA-T is a fully thin-film, high-performing power generation and communications array for small spacecraft. Inherently, small spacecraft are small where mass, volume, and surface area are extremely limited resources. Small spacecraft technologies and capabilities are rapidly progressing, which is beginning to make them an attractive option for scientific, exploratory, and commercial interests. However, the small spacecraft power generation system is lagging. Many in the community are asking for more electrical power, and with more power, more mission capability will come. Traditionally, more power equates to larger solar arrays – leaving little allocation remaining for payload. Herein, recent advancements of the LISA-T small spacecraft thin-film power generation solution are presented. Updates to the advantageous integration of antenna elements on the power generation array are discussed. Benchtop deployment testing is detailed alongside environmental testing, culminating in a classification of TRL-6.

[*] Deputy Center Chief Technologist, NASA MSFC Science and Technology
[†] Solar Sail Principal Investigator, NASA MSFC Science and Technology
[‡] Wireless Engineer, NASA MSFC Engineering Systems
[§] Environmental Test Engineer, NASA MSFC Engineering Materials
[**] Materials Engineer, NASA MSFC Engineering Materials
[††] Director, NeXolve Holding, LLC Advanced Materials
[‡‡] Chemist, NeXolve Holding, LLC Advanced Materials

Introduction

SATELLITE miniaturization continues to create lower cost, faster paced, higher risk tolerant for space missions. Small spacecraft – defined here as spacecraft less than 180kg – continue to grow in popularity and are becoming of interest to scientific, exploratory, and commercial missions alike. The large body of research and development within government, academia, and industry has greatly advanced small spacecraft technologies and, as a result, mission capabilities. However, electrical power systems have not commensurately increased in capability, creating a bottleneck in bus design and, ultimately, payload capability. This drives the need for advanced power generation, storage, and distribution designs.

An important class of small spacecraft is the well-known CubeSat. Since their conception, CubeSats have quickly progressed from educational tools to scientific, exploratory, and commercial contributors. Herein, CubeSats will be used as reference spacecraft, but the concepts are transferrable to other small spacecrafts. CubeSats typically utilize either body mounted or deployable solar panels for power generation. Body mounted panels can supply in the range of 2.25W/U when utilizing triple-junction III-V solar cells. Here, 'U' denotes a single CubeSat unit of ~10x10x10cm. Though they supply low power levels, body mounting is mechanically simple and can supply 2-axis+ of power generation – relaxing the solar pointing requirement. To reach higher power levels, several impressive deployable options exist. 3, 6, and 12U designs can reach power levels of 35 to 100W+. Though these arrays could be scaled to provide even higher power levels, the mass, volume, and surface area required to do so would greatly restrict bus resources and the payload they are trying to power. To achieve higher power generation while maintaining significant resource allocation for the payload, NASA is adapting traditional solar array materials and their supporting deployment mechanisms to utilize thin-film solar cells, lightweight polyimides, and compact mechanical mechanisms to do more from less.

The use of thin-film based solar arrays for spacecraft applications has long been recognized as an advantageous power generation option.[1-7] Thinner materials yield mass savings, equating to lighter launch loads and/or more payload allocation. Perhaps more importantly for small spacecraft, their mechanical flexibility lends itself well to stowage and deployment schemes. These benefits make thin-film arrays an exciting prospect for small spacecraft. Though several larger scale thin-film or partial thin-film arrays are in development, sub-kilowatt thin-film arrays – optimized for small spacecraft – remain in need. NASA's Lightweight Integrated Solar Array and Transceiver (LISA-

T)* is addressing this – greatly enhancing power generation and, as will be discussed further below, communication capabilities for small spacecraft.

3rd Generation Advancements

Early design concepts and testing of the LISA-T array have been previously published.[8-10] LISA-T is currently being developed in two configurations to support different mission needs: (a) planar and (b) omnidirectional. The planar array is a spacecraft pointed design geared towards high power, high performance applications. The omnidirectional array is a GN&C (guidance navigation and control) simple design which allows constant power generation and communication coverage for tumbling spacecraft or spacecraft pointing/slewing at targets other than the sun and communication locations. Both configurations utilize >95% of the same design and hardware, differing only the method and the angle at which the petals are locked out.

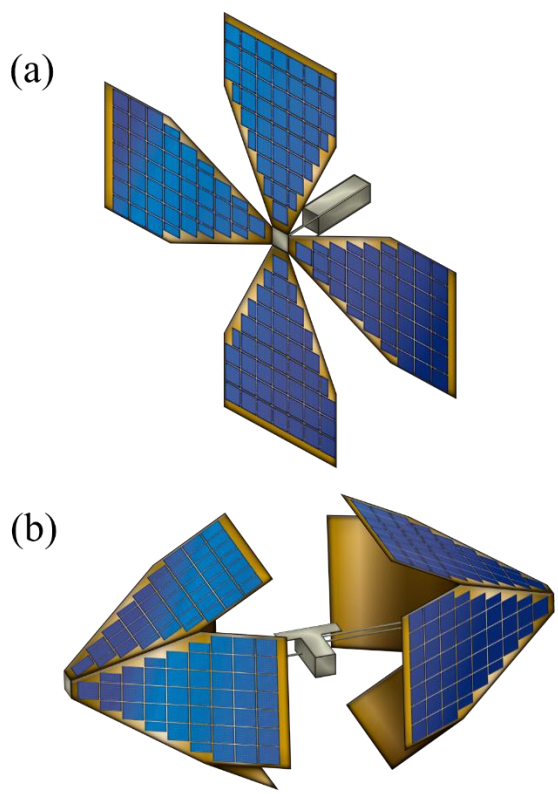

Fig. 1 Depictions of LISA-T (a) planar and (b) omnidirectional array configurations.

Central Deployment

NOTEL: * LISA-T, Originally named Lightweight Integrated Solar Array and Transceiver has been renamed Lightweight Integrated Solar Array and anTenna

At the core of the array is the central deployment mechanism (**Fig. 2**). This mechanism is an adapted version of the Air Force Research Laboratory's SIMPLE (self-contained linear meter-class deployable)[11] design. The deployment enables the petal stack to be pushed away from the host bus. This is necessary for the omnidirectional configuration, which requires this clearance to properly form the geometry. It is, however, optional for the planar configuration. Central deployment can be used with the planar configuration to increase thermal view, payload view, or the like. The planar configuration can also be deployed directly off the host bus without central extension (as will be shown in **Fig**. 7). Bistable fiberglass layup 'tape springs' are being utilized for the central booms. The bistable booms roll tightly for stowage and passively deploy *via* stored strain energy. A Dyneema® tie down restrains the booms for launch and a thermal knife releases the tape booms on orbit.

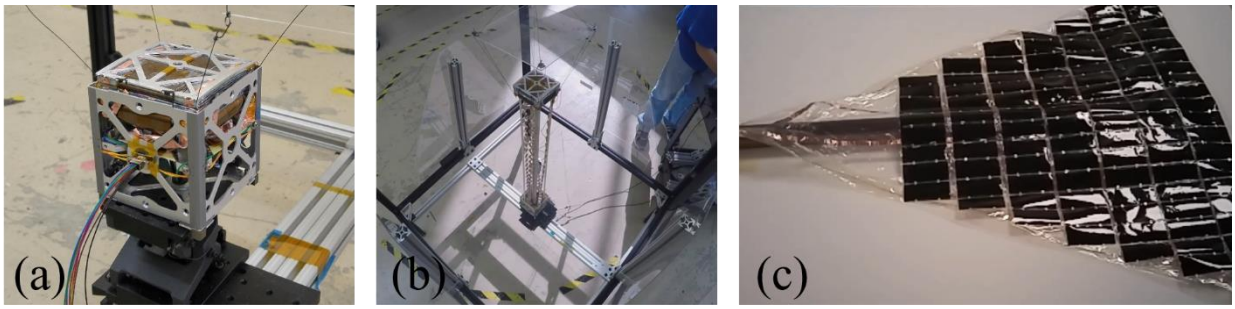

Fig. 2 Generation 3 LISA-T hardware, (a) stowed, (b) central deployed, and (c) sample petal.

The petal stack is a tightly packed fold-up of the solar cells, substrate, coatings, and multicomponent panel deployment and structural system. There are four solar cell petals in both configurations.

Solar Cell Petal

Each petal is built on a toughened colorless polyimide 1 (T-CP1) substrate. This material is a stronger, tear-resistant version of NASA's well known solar sail material, CP1™; which produced by NeXolve Holding Company.[12, 13] The team utilizes lessons learned from NASA's solar sail development in the design and fabrication of theses petals.[14, 15] Thin-film solar cells are embedded in the substrate, *without* the use of an additional adhesive. This gives the thinnest stack possible, reduces mass, and reduces the risk of delamination from CTE (Coefficient of Thermal Expansion) mismatch between the substrate, adhesive, and solar cell. The solar cells are electrically interconnected with thin-film silver ribbon, which is welded from cell to cell. String power is routed via copper ribbon embedded – without adhesive – into the T-CP1 substrate. To ensure electrical insulation, both the interconnects and power busses are encapsulated with T-CP1. 4th generation interconnects and power busses will be encapsulated with NeXolve's new

toughened CORIN®XLS (Colorless Organic Inorganic Nanocomposite)[13, 16] to also provide atomic oxygen resistance to the encapsulated parts. In the 3rd generation prototype, petals were fabricated from both copper indium gallium (di)selenide (CIGS; Ascent Solar) as well as inverted metamorphic multijunction (IMM; Microlink Devices, Inc.) thin-film solar cell technologies. **Table 1** summarizes the solar cell properties. Note, the mechanical systems have been designed to a unit cell size (~9x9cm); meaning, the petal is largely cell agnostic so long as the solar cell or multiples thereof can be fit into the unit cell size.

Table 1 Summary of LISA-T employed thin-film solar cells.

	CIGS	**IMM**
Efficiency (AM0)	10.5 %	25%*
Cell Size	8.6 x 8.6 cm	6.6 x 3.0 cm
Cell Voltage	6.2 Voc	2.9 Voc
Cell Current	0.22 Isc	0.28 Isc
Cell mass	110 g/m^2	250 g/m^2

*Note: the IMM cells are available at higher efficiencies.

Petal voltage and current characteristics are flexible to fit mission needs. As examples, the CIGS 3rd generation petals were strung to support a typical 28V bus while supplying ~1.25A_{mp} at peak power (~34.0W) per petal. The IMM petals were strung to show higher voltage operation, ~52.5V_{mp} and ~1.10A_{mp} at peak power (~57.7W) per petal. The four IMM petals can then be strung together to provide >200V_{mp}. 3rd generation petals did not incorporate blocking nor bypass diodes. 4th generation petals, which are currently in development, will begin including both diode types.

The cells are encapsulated with a flexible polymer to provide environmental protection from moisture uptake, atomic oxygen, low energy particulate radiation, and the like. Several potential coatings, both with and without experimental loadings of cerium oxide (ceria), were studied under simulated space environments; the results are presented below. The key characteristic for these coatings in this application is that they are solution processable through a range of thicknesses, negating the need for adhesive. The 3rd generation petals utilized 0.5 to 1.0mil thickness coatings. It will be detailed below that the exact ultraviolet clarity of the cover is important for the different cell technologies. Further, the cover thickness is also important for both the radiation environment as well as atomic

oxygen erosion. In future applications – such as those requiring much thicker but flexible covers – other coatings, such as pseudomorphic glass,[17-19] could be employed.

A multicomponent support and deployment structure form the mechanical basis of the petal. The structure both unfolds the petal web as well as holds its deployed shape, while still allowing it to be folded and stowed compactly. The system is comprised of two key components: Elgiloy® c-booms and a shape memory wire matrix. **Fig.** 3 shows pictures of the backside-mounted deployment and structure backbone a CIGS petal. Note, the same structure was used for both CIGS as well as IMM petals and designed around the unit cell size. Elgiloy® booms form both a central mast and spar boom. For added stability, the mast forms a full circle near the root, where the petal connects to the deployment plate. Farther down, the mast forms a half circle or a 'C' with strategically spaced collars to maintain its offset and complete its length. The spar booms are also formed from a 'C' with evenly spaced collars. Both the mast and spar booms give the system deployment force as well as support structure. Both the Elgiloy® boom deployment and support are passive, that is, they do not require any active input. However, the booms themselves do not induce enough force to completely unfold the petals. A shape memory alloy (SMA) wire matrix is also embedded on the backside of the petal. Its pattern is subtle in the figure but can be identified by the serpentine lamination of the nickel-titanium wire. The SMA, which is activated by heat, gives a strong, active deployment force for unfolding the petals.

Fig. 3 Backside 3rd generation CIGS petals.

Antenna Integration

Integrating solar generation and communication capability on the same deployable is known to be an advantageous configuration. This integration has the potential to reduce bus space and mass claim while creating opportunities for

higher gain design, spherical coverage communications, and electronically steered arrays. In generation one, custom UHF (Ultra High Frequency) and S-band antennas were utilized. UHF dipoles were fabricated with flexible copper ribbon and integrated directly on the backside of the array panel. S-band patches were also included by mounting directly to the chassis and/or deployed plates. In generation two, the antennas were matured to utilize thermally set super elastic nickel-titanium wire. Both UHF dipoles as well as S- and X-band axial helixes were fabricated. The axial helical antennas compress during stowage and self-extend upon release. The UHF antennas were again directly embedded on the back of the array. The early S/X helical antennas were embedded on the front side of the array, in place of a single cell or on the deployment plate structure. In the third-generation development, the helical structure and fabrication were matured and their placement on the LISA-T array was refined to fit different mission scenarios.

Fig. 4 Sample 3rd generation nickel-titanium helical antennas (a) S-band and (b) X-band array.

The maturation of the helical antennas included more precise shaping of the helical structure, improved soldering techniques, improved insulation from the ground plane, and increased structural stability for the S-band design. Computational simulations show a gain of 10 dBi with a 47-degree beam width. Center frequencies have been simulated and verified via return loss measurements. Radiation pattern testing to further verify simulated results is planned in the future. With passive deployment, the antennas have a stowage thickness of approximately 0.7 mm. The mass of these antennas is approximately 10 grams. These characteristics make them an ideal match for integration into the lightweight solar array.

By strategically placing multiple antennas in place of a solar cell or on the top deployment plate, spherical coverage can be achieved. If a lower gain antenna meets mission needs, S and X band edge fed and direct fed circular patch slotted antennas on 62 mil Duroid have also been designed and simulated. These antennas have a simulated gain of around 7 dBi and are significantly thicker, with greater mass; however, they have a simulated beam width of 78 – 81 degrees which provides better spherical coverage.

For planar solar array configurations, the passive deploying axial helical antennas can similarly be placed on the deployment plate or in the place of a solar cell – providing pointed, high gain communication. This is especially useful for deep space applications where the antenna is on same face as the solar array to minimize slewing.

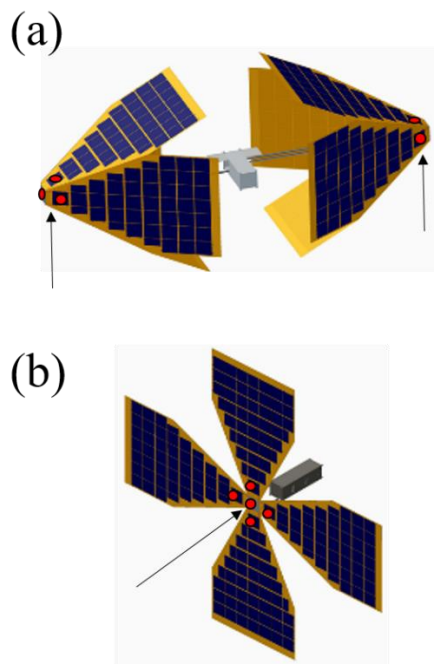

Fig. 5 Placement locations for integrated antennas to provide (a) spherical coverage and (b) high-gain pointed communications.

Ka-Band helical antennas were also fabricated in the 3rd generation prototyping (**Fig. 6**). These antennas were fabricated from an alloy of copper-beryllium to enable a wider range of operational temperatures. During environment testing, the S band helical antennas demonstrated a transition of the super elastic nickel-titanium to a softer state at low temperatures around -5 degrees Celsius. This was visibly observed as the helical wire began to slightly lose form under the force of gravity. In a space environment, the softening of the wire is theorized to have negligible effect, especially on the smaller X band antennas with a higher wire thickness to helix size ratio. Once the temperature was raised, the set shape was once again restored. Sending a current through nickel-titanium has been demonstrated to raise its temperature. Therefore, sending a signal to the antenna should restore or prevent deformations. Further testing is needed to verify.

To alleviate this risk, the latest generation of antennas use a copper-beryllium alloy instead of nickel-titanium. This alloy has a much lower transition temperature. X band and Ka band prototypes have been constructed using this copper-beryllium alloy and simulated to verify similar performance.

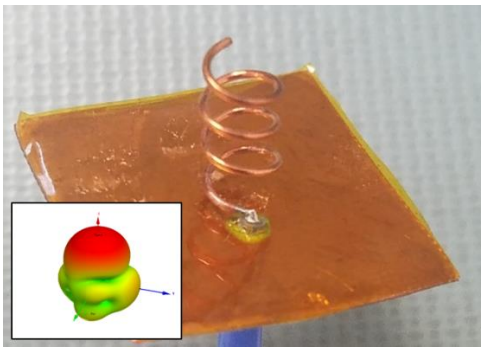

Fig. 6 LISA-T Ka-Band helical prototype. The insert shows the simulated performance with 14.2db (GainRHCP) in red, -7.4dB in yellow, and -26.3dB in green.

Benchtop mechanical and electrical testing

Both the omnidirectional and planar arrays were deployed in a gravity offload test rig to show mechanical operation. CIGS based petals were utilized for the full-up benchtop testing. **Fig. 7** shows the sequence of a planar LISA-T benchtop deployment from stowed through completed unfolding.

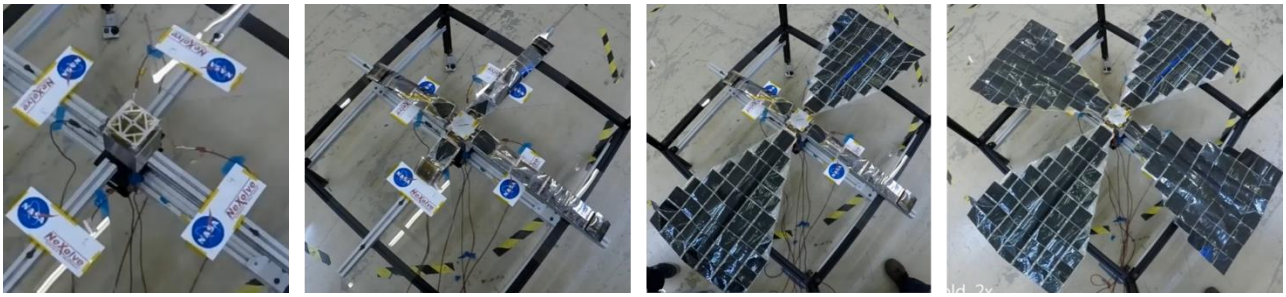

Fig. 7 Sequence of planar LISA-T benchtop deployment.

Neither the antenna nor central deployment mechanism were included on this test article, however, both can be included per mission requirements. Pane 1 shows the petal stack stowed on the host 1U. The petal release mechanism was activated to deploy the mast booms (pane 2). Note that each boom passively deployed to a different length. This

was likely caused by a varying degree of wear on the booms and the nuances of where they were caught by the gravity support plates. Nonetheless, it highlights the power of the SMA wire, which when activated, fully unfolded each of the petals in 1g – no matter how far they had passively deployed during mast release. Pane 3 shows after two petals were unfolded and pane 4 shows the completed, successful deployment.

Fig. 8 shows the sequence of an omnidirectional LISA-T benchtop deployment from stowed through complete unfolding.

Fig. 8 Sequence of omnidirectional LISA-T benchtop deployment.

Both the antenna (array of 4x 10dbi x-band Helicals) and central deployment mechanism (0.75m) were included. Only a single side of the array was deployed due to gravity offload restrictions. The first row of panes shows the central deployment. Release mechanism one is activated to release the strain energy of the central tape booms. Once completed, release mechanism two is then activated to release the mast booms. This is the same activation as the initial panes of the planar array (Fig. 7), however, the petals release to lock at -60º as opposed to 0º in the planar case. The final panes show the SMA unfold all the omnidirectional petals.

A double sided, mass simulator benchtop deployment was also performed to ensure the mechanics and kinematics of the dual sided omnidirectional array. The dual sided deployer was hung from a ball bearing rod via springs. This enables the high degree of freedom of motion to watch kinematics. Mass simulators for each petal stack were included (copper on ends of deployer) as was a mass simulator for the spacecraft bus (stainless below central mechanism). The deployment was smooth with only minor movement occurring during lockout. A slight twist was noted on the right side of the tape booms near the end of the deployment; however, the mechanism easily righted itself.

Benchtop deployment of the IMM petals were also performed. **Fig.** 9 shows the deployment sequence. No major differences compared with the CIGS petal deployments were noted.

Fig. 9 Sequence of LISA-T IMM petal benchtop deployment.

Both petals were tested under AM0 (Air Mass Zero) via a calibrated Large Area Pulsed Solar Simulator (**Table 2**). The petals were tested after coating and laydown without deployment structure ('web only'), then again after the deployment structure was added. A 2 and 9% loss for the CIGS and IMM respectively was noted. A majority of the loss stems from the curvature and wrinkles the deployment system imparts on the petal web. A further ~8.5% was lost after deployment on both petal types. Curvature and wrinkling are worse after stow/deployment as compared to a freshly made petal. Further, slight damage to a subset of the cells has now been ruled out and is under investigation. Nonetheless, even with these losses, the LISA-T design achieves a large improvement to state of the art.

Table 2 Electrical, mass, and thickness characteristics of the LISA-T CIGS and IMM petals.

	CIGS Petal	**IMM Petal**
Petal power 0° web only	37.3W	69.3W
Petal power 0° web + deployment structure	36.6W (98.1%)	63.1W (91.1%)
Petal power 0° after deployment	33.5W (91.5%)	57.7W (91.4%)
Petal 30° side view	29.4W	50.4W
Petal 60° top view	15.9W	27.3W
Petal mass	111g	130g
Petal thickness (stowed 9x9cm)	0.70cm	0.95cm

Performance Metrics

Table 3 summaries the performance of the prototyped Planar and Omnidirectional LISA-T Arrays. Masses and stowed volume include the entire array from cell through deployment system, electrical connectors and the like. The planar array is likely scalable between 50 and 500W with similar performance metrics. Further, lower efficiency IMM

cells (~25% AMO) were utilized for this demonstration; further performance gain could be achieved with the higher efficiency IMMs currently available (>30% AM0).

Table 3 Array level performance metrics of the Planar and Omnidirectional LISA-T Arrays.

	IMM Array	**CIGS Array**
Planar		
Array power generation	230.9W	134.0W
Array stowage volume	461.8kW/m^3	340.0kW/m^3
Array mass	378.5W/kg	250.9W/kg
Omnidirectional		
Array power generation	101.0W	60.0W
Array stowage volume	101.0kW/m^3	60.0kW/m^3
Array mass	75.7W/kg	47.8W/kg
Generation axes	3-axis	3-axis

Note: Planar array likely scalable between 50 and 500W with similar performance metrics.

TRL-6 Testing

The design discussed above has been preliminarily tested through a Low Earth Orbit (LEO) relevant exposure to achieve Technology Readiness Level (TRL) 6 in this environment. Though the number of tested samples remains low, this preliminary testing indicates good survivability for the typically shorter term (<1 year) mission life of small craft. This test data also gives good indication as to the weak points in survivability and should drive focus of future materials development for longer lifespan.

The operational and relevant testing environment was defined as follows.

On-Ground: It is assumed that LISA-T will be launched from NASA Kennedy Space Center (KSC) in Cape Canaveral, FL. While waiting for launch, the LISA-T flight article may be subject to extended periods of time in the stowed configuration (in a controlled environment). Further, during pre-launch the stowed article may wait on the pad for a short period of time (nominally <10days) and, depending on the mission configuration, be exposed to elevated temperatures and relative humidity. Both humidity exposure and extended stowage are defined as TRL6 relevant environments.

Launch: During launch, payloads are subject to high vibrations which can shake loose mechanisms and attachments and possibly shift components. Also, during launch, residual trapped gasses in the solar array folds and booms must be able to vent during booster ascent without causing any damage or disturbances to the stowed configuration. Ascent vent was defined as a TRL6 relevant environment; however, launch vibration is to be analyzed and tested during the TRL7 campaign as specific launch vehicles are narrowed. (Note, future test campaigns mimicking the path of the LISA-T testing should consider vibrational analysis and test *during* TRL6 utilizing the GEVS (General Environmental Verification Standard) document).

On orbit (6 months LEO): LISA-T has been designed with an initial target of 6 months in low Earth orbit (LEO) at approximately the International Space Station (ISS) altitude (~400 km). While reentry analysis indicates that the large area, low mass ballistic coefficient will likely deorbit a passive LISA-T spacecraft from 400 km before 6 months, the ISS environment is well defined and represents a good starting point for test and analysis with regards to environmental exposure and survivability. The ISS also houses a materials testing platform, MISSE-FF (Materials on International Space Station Experiment – Flight Facility), which is being used to corroborate LISA-T ground testing. The ISS LEO environment is characterized by: high vacuum, high density plasma, neutral atomic oxygen, particulate radiation, thermal extremes and cycling, and ultraviolet radiation exposure. All were defined as TRL6 relevant environments except for the high density plasma. The adverse effects of plasma induced arcing on solar arrays are known to be benign when the array is operated in a 'safe' voltage-current zone.[20] LISA-T is currently being assumed to be operated in this zone.

Table 4 Summary of the TRL6 test campaign; including the benchtop deployment detailed above.

Environment	**4-petal**	**1-petal**	**Sub-coupon**	**CIGS**	**IMM**	**Exposure**
On ground:						
Extended stowage		x		x		15 days stowed
Humidity exposure			x	x		10 days @ 80%RH 27°C
In launch:						
Ascent vent	x			x		Pump down to $1E^{-6}$torr, deploy
In orbit (6 months ISS):						
High vacuum		x	x	x	x	Indirectly test throughout other experiments

Neutral atomic oxygen					x	2.5E21atoms\cm^2
Particulate radiation						
Electron				x	x	1MeV @ 3E13-5E15e$^-$/cm^2
Proton				x	x	50, 100, 500, 700keV @ 7E10-1E15p$^+$/cm^2
Thermal extremes and cycles			x	x	x	750 cycles -68°C to +117°C, 750 cycles -118°C to +7°C, 8 extreme cycles -118°C to +117°C
Rapid thermal cycling			x	x	x	100cycles -55°C to +125°C
Thermal vacuum deployments		x		x		±40°C deployments
Ultraviolet radiation				x	x	>2,000 UV equivalent sun hours
Benchtop deployments:						
Omnidirectional configuration	x			x		Benchtop full function deployment
Planar configuration	x			x		Benchtop full function deployment
Single petal		x		x	x	Benchtop deployment

Extended Stowage

Prototyping and benchtop testing was done with a quick stowage to deployment turnaround. Typically, the article was stowed in the morning and deployed in the afternoon – remaining stowed for only an hour or two. At most, stowage went overnight. In application, however, it is likely that the article would remain stowed for an extended period of time. At the least, 14 days of stowage are expected in order to accommodate launch vehicle integration and launch delay margin. Depending on the exact mission, primary payload, and the like, shelf life may need to be 3 months or greater. Extended stows pose a risk as the deployment elements are stowed under strain. This can induce creep, relaxation, or other effects that may reduce or otherwise alter the boom deployment characteristics. Initial extended stow experiments have been conducted on both the central boom mechanism as well as the petals. In both cases, fully deployed [unstrained] hardware was kept next to stowed [strained] counterparts for 15 days. The fully deployed hardware was then stowed and immediately deployed. Subsequently, the 15-day stowed article was deployed and the two were compared. No noticeable difference was found. The 15-day petals, however, exhibited a slower deployment that relied more on the active SMA to unfold. Meaning, the 15-day petals held somewhat tighter after

release, with less passive unfolding from the Elgiloy® booms – perhaps indicating some relaxation of the booms. Nonetheless, once the SMA was activated the petal was fully unfolded and held its shape without issue. Longer extended stow experiments (>3 months) are currently underway.

Humidity

Moisture uptake, especially at elevated temperatures, can reduce solar cell output by oxidizing electrical components such as metal gridline and cell to cell interconnects. To understand this potential degradation, LISA-T sub-coupons were exposed to ~80% relative humidity (RH) @ ~27°C for 10 days – representing a mean exposure in the Cape summertime. CIGS base sub-coupons were prioritized as they were known to be most sensitive to moisture and oxidation. Both bare and coated CIGS cells were exposed directly to the humid environment (Thermotron SM-8-8200 Environment Test Chamber) in a deployed state. This was a worst case condition as a flight article would be exposed in a stowed state – folded with Elgiloy® booms and sandwiched between a top hat and bread plate. The stowed state will inhibit moisture absorption, further protecting the cells.

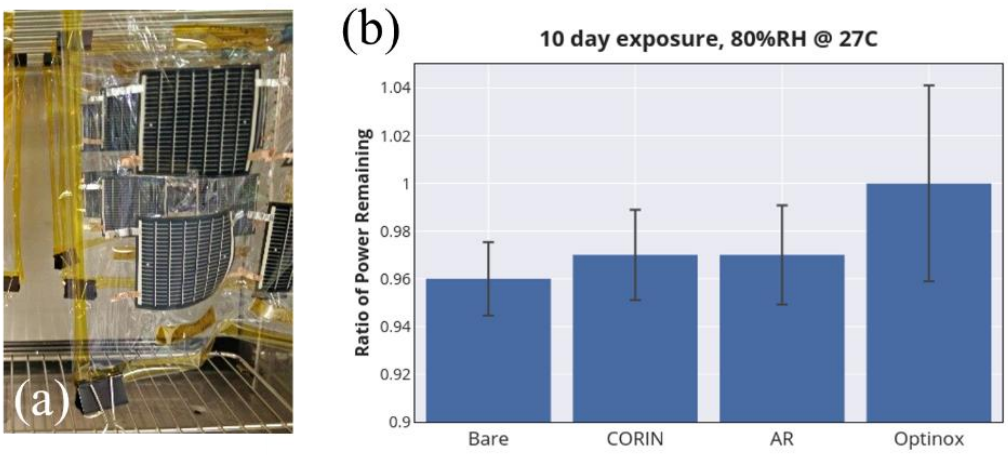

Fig. 10 Humidity exposure experiment: (a) CIGS sub-coupon under test and (b) CIGS power remaining after exposure.

Fig. 10 summarizes the deployed state CIGS sub-coupon humidity exposure experiment. Three cells were averaged per data point. Bare cells retained ~96% power output. The CORIN®XLS and Optinox®SR[21] coatings gave protection at ~97% and ~100% retention respectively. Material properties do not account for this variance as no difference in moisture absorption between the different coatings is expected. It is likely the difference stems from subtle fabrication differences – the straight Optinox®SR coating was slightly thicker than expected. Nonetheless, the

results indicate that even the deployed assemblies can withstand exposure to the hot-humid environment while awaiting launch. Both the IMM cells as well as the more realistic stowed state exposure are expected to perform better, further strengthening the indication of functionality in this environment.

Ascent Vent and Thermal vacuum deployments

To ensure trapped gasses in the array folds and booms could properly vent during launch ascent, a vacuum deployment test was conducted. The array was stowed, pumped to 10^{-6} torr or better, and subsequently deployed. The pump rate was not directly controlled, but 10^{-6} torr was reached in ~1.5 hours. **Fig.** 11 shows the high vacuum deployment – no damage or deployment issues were introduced by the vent.

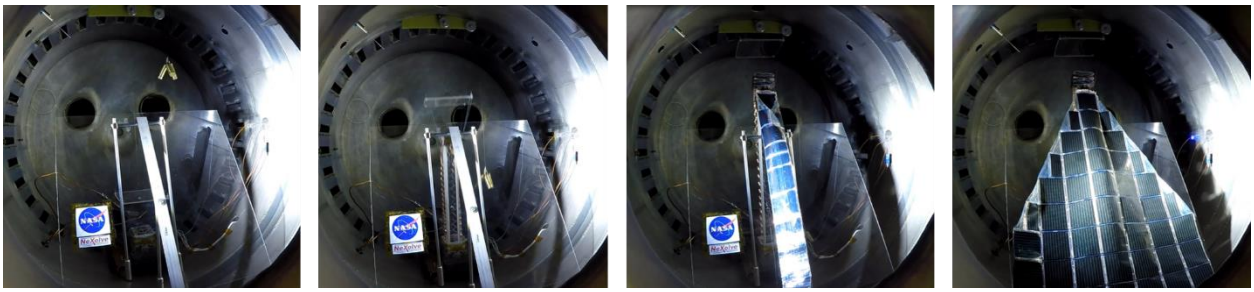

Fig. 11 Progression of High Vacuum LISA-T Deployment.

The vacuum deployment testing was then repeated at both hot and cold cases. The central boom and petal deployments were tested separately (**Fig. 12**) to enable better temperature control of the critical components. ±40°C or better were successfully tested for both the central boom and petal, showing deployment at temperature extremes within the spacecraft bus is possible. Of particular interest is the noted trend of slowing deployment with cooling of central booms. From ~20°C to ~-40°C the time to full deployment nearly doubled, indicating a decrease in deployment force. It is suspected that with low enough temperatures a 'freeze out' would occur and the deployment could be hindered. The data also indicates the same is true with high temperatures; there may be relaxation of the fibers, again slowing deployment and eventually completely hindering it. More investigation is needed at higher temperatures, however, in current mission designs it is unlikely deployment would occur >50°C.

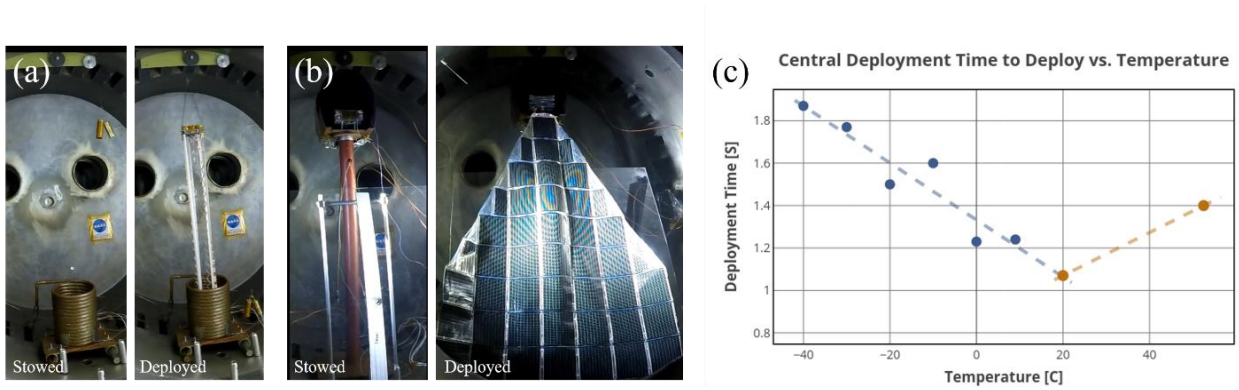

Fig. 12 Hot/Cold vacuum deployment of LISA-T (a) central boom and (b) petal. (c) Deployment time trend of cold booms.

Above 40°C the petal SMA needs to be considered. The current alloy being employed has an austenite phase transition around 50°C. Meaning, the SMA will begin to unfold around this temperature. Higher temperature alloys exist and can be employed depending on mission requirements.

Neutral Atomic Oxygen

To simulate six months at ISS under solar maximum, coated and uncoated solar cells as well as bare cover materials were exposed to ~2.4E21 atoms/cm^2 neutral atomic oxygen (AO). Free films of CORIN®XLS with and without ceria, Optinox®SR with and without ceria, alongside Kapton® witnesses as well as bare IMM cells alongside CORIN®XLS coated cells were tested (**Fig. 13**).

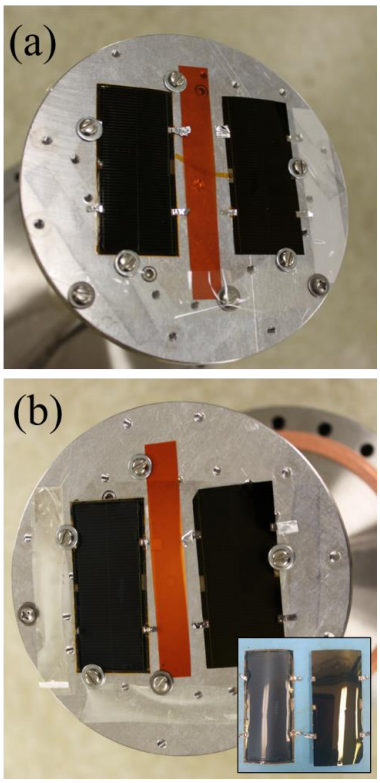

Fig. 13 IMM Neutral atomic oxygen experiment (a) before exposure and (b) after ~2.4E21 atoms/cm^2; the insert shows more direct lighting and the hazing on the CORIN®XLS IMM cell.

Table 5 summarizes the free film material loss results. Optinox®SR samples reacted significantly with the AO. Pure Optinox®SR retained just 29% of its mass, with some areas completely eroded after just ~2months ISS solar maximum equivalent exposure. This equates to an erosion yield of ~3.24E-24cm^3/atom. Interestingly, the addition of ceria significantly improved the film, retaining ~76.5% mass – an erosion yield of ~1.05E-24cm^3/atom. The ceria loadings were included in the coatings to mimic gains noted in the traditional ceria-stabilized microsheet and other glasses where the addition of small percentages (1-2%) has been found to prevent the formation of color centers during exposure to particulate and ultra violet (UV) radiation.[22, 23] Ceria may also be an advantageous addition for AO erosion yield. Further investigation is underway. As expected from previous MISSE exposure, CORIN®XLS performed well, retaining >96% of its mass. During round 2, the yield was measured at 9.33E-26cm^3/atom. The round 2 CORIN®XLS samples were also exposed during round 3; the erosion rate slowed to 3.98E-26cm^3/atom, for an overall yield of 6.56E-26cm^3/atom through 1.5E21atoms/cm^2. This slowing is expected as the CORIN®XLS forms a self-passivating layer when exposed to AO, reducing the progression of erosion. The measure yield is in line with

MISSE-6A ram data which showed an erosion rate of 8.4E-26 cm^3/atom for ~2.0E21atoms/cm^2 exposure. The addition of ceria did not have a further effect on the CORIN®XLS film.

Table 5 Summary of free film material loss during neutral atomic oxygen experiment.

	Pre	**Round 1: 8.1E20 atoms/cm^2**	**Round 2: 7.5E20 atoms/cm^2**	**Round 3: 7.6E20 atoms/cm^2**
Run 1				
CORIN®XLS CERIA	0.0161g	0.0144g		
Optinox®SR	0.0579g	0.0168g		
Optinox®SR CERIA	0.0625g	0.0478g		
Kapton® witness	0.2161g	0.1561g		
Run 2				
CORIN®XLS CERIA	0.0107g		0.0097g	
CORIN®XLS CERIA	0.0124g		0.0113g	
CORIN®XLS	0.0326g		0.0314g	0.0309g
Kapton® witness	0.1962g		0.1497g	
Run 3				
CORIN®XLS	0.0335g			0.0323g
Kapton® witness	0.1968g			0.1500g

Fig. 14 depicts the bare and CORIN®XLS coated cell data. In **Fig**. 13b, a slight hazing can be noted on the CORIN®XLS cell. This is likely due to an irregular surface caused from AO erosion of the film surface and an increase in light scattering. Transmission data through the free CORIN®XLS films showed a broadband reduction between ~290 and 2300nm; some wavelengths losing as much as 60% [absolute]. Optical data on the CORIN®XLS coated cell showed a reduction (1-10% [absolute]; -2.3% [absolute] on average) in reflection, most prominent for wavelengths >680nm. Reflection on the bare IMM cell was essentially unchanged. The power retention data (**Fig**. 14) shows clears trends for both the bare and coated cells. The bare cell showed a decline through the exposure, losing ~2.4% from max power. This is likely due to oxidation of topside collection grid and tabs. Interestingly, the CORIN®XLS cell improved through the exposure, gaining ~3.6% in max power. It is possible that this stems from increased light

coupling – originating from the increased light scattering and decreased reflections. The peaks and valleys that are generated during the AO erosion may act in the same way as an antireflective coating. More AO exposures with correlation to on-orbit data of LISA-T assemblies are needed.

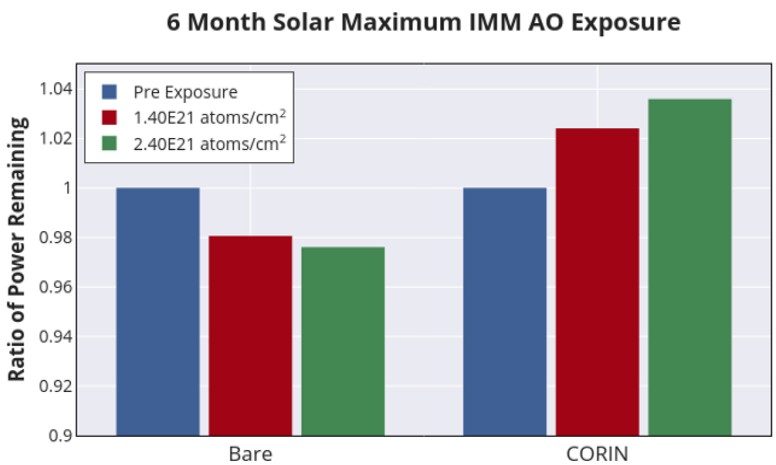

Fig. 14 Neutral atomic oxygen data for Bare and CORIN®XLS IMM solar cells.

Particulate Radiation

To predict solar cell survivability in a particulate radiation environment an equivalent dose model is used. The damage done by a charged particle of a particular energy is referenced to the damage done at a base energy via a damage coefficient. This base energy can be 1 MeV electron for both charged electrons and protons or, alternatively, 1 MeV electron for charged electrons and 10 MeV proton for charged protons. Modelling software such as SPENVIS can mine the AE and AP radiation models to determine the '1 MeV equivalent electron dose' (or 1 MeV equivalent electron + 10 MeV equivalent proton dose). The cell assembly in question can then be tested at this equivalent energy to create a fluence degradation curve that will predict on-orbit degradation. Though the modeling software does not yet contain information for the thin-film junctions being used by LISA-T, it is likely the damage mechanisms are similar and that the state of the art models can give initial insight into LISA-T assembly survivability. To form a basis of particulate radiation testing, LISA-T assemblies were exposed to 1 MeV electron testing through a sweep of fluences. Further, the assemblies were also exposed to low energy protons (50 keV, 100 keV, 500 keV and 700 keV) to test the stopping power of the thin-film coatings.

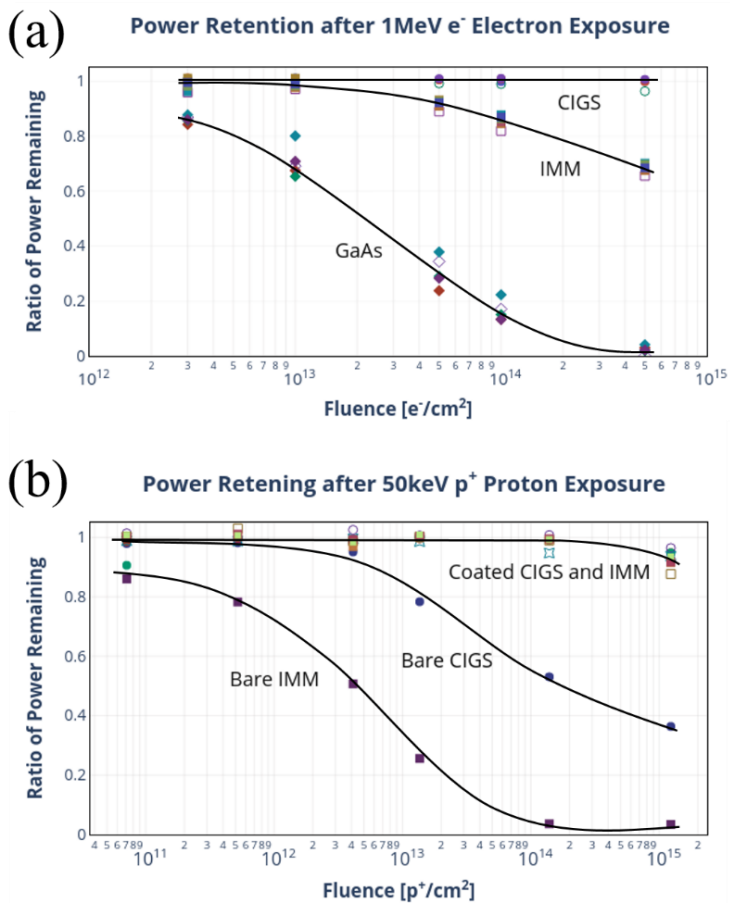

Fig. 15 Power retention of LISA-T cell assemblies after (a) 1MeV e^- electron and (b) 50keV p+ proton exposures.

Fig. 15 shows the fluence degradation curves of the LISA-T assemblies in both 1 MeV electrons and 50 keV protons. Two cells from two different radiation runs are averaged per data point. Each color in the cell groupings represents a different coating; bare cells alongside CORIN®XLS, CORIN®XLS with ceria, Optinox®SR, Optinox®SR with ceria, anti-reflective Optinox®SR, as well as cell backsides were exposed. Exposures were run with a target of 9.0 nA/cm^2 flux for electrons and 1.0 nA/cm^2 for protons. Note, candidate single junction GaAs (Gallium Arsenide) assemblies are included in the electron data. These assembly types were not tested throughout the other environments; however, as will be discussed, they are included in the on-going on-orbit exposure experiment. Perhaps most apparent in the electron data (**Fig**. 15a) is that each assembly type is tight; meaning, the various coatings had little effect at these energies. And, more importantly, *vice versa*. Free films of the coating materials were also exposed. No significant difference in optical properties was seen. The CIGS assemblies showed little change throughout the fluences, highlighting their fairly well known radiation tolerance.[24, 25] The IMM assemblies showed a more average

degradation curve, underperforming their thick-film III-V counterparts, but showing reasonable radiation tolerance – especially for shorter term small spacecraft missions. The single junction GaAs somewhat lagged. However, it should be noted that new formulations exist, which are expected to have greatly improved radiation stability.

For context, a sample 1 MeV equivalent dose model was generated utilizing SPENVIS (AE8/A9, EQFLUX) for triple junction, thick-film SOA (State of the Art) III-V cells at 400 km, 63.4° inclination over 6 months. Even a bare SOA would receive an equivalent 1 MeV electron dose of only ~3.6×10^{13} e-/cm^2. With a traditional 0.25 mil coverglass (approximate equivalent protection as 0.5 mil LISA-T polyimide), the fluence is reduced further to ~1.2E12e-/cm2 as lower energy particles are blocked – indicating radiation survivability solutions for all cell type assemblies.

The most damaging particulate radiation comes from low energy charged particles which embed themselves within the solar cell active material, especially near the semiconductor junction. The higher energy particles (e.g. 1 MeV electrons) move through the entire thickness of the cell, distributing energy/damage linearly. Low energy particles, however, create non-uniform damage – making their applicability to the equivalency model difficult. 50-100 keV protons are known to be some of most damaging for SOA cells. In fact, proton energies as high as 1MeV are stated to be non-linear. To ensure the LISA-T cell assembly 12.7 to 24.4 µm polyimide coatings can shield the cells from these damaging particles without significant degradation, the assemblies were exposed to 50, 100, 500, and 700 keV protons.

Fig. 15b shows the 50 keV p+ exposure through a fluence sweep. For both cell assemblies testing, the LISA-T coatings provided significant protection. All coatings gave similar stoppage power, greatly protecting power output when compared to the bare, uncoated cells. To determine the energy cut-on for the LISA-T cell coatings, the proton energy was then stepped up to 100, 500, and 700 keV with a constant 1×10^{13} p$^+$/cm^2 fluence (**Fig. 16**). Both 0.5mil and 1 mil coatings were tested. Significant protection was seen through 700 keV, indicating strong stopping power through these energies. First order calculations predict stopping ability up to ~800 keV p$^+$.

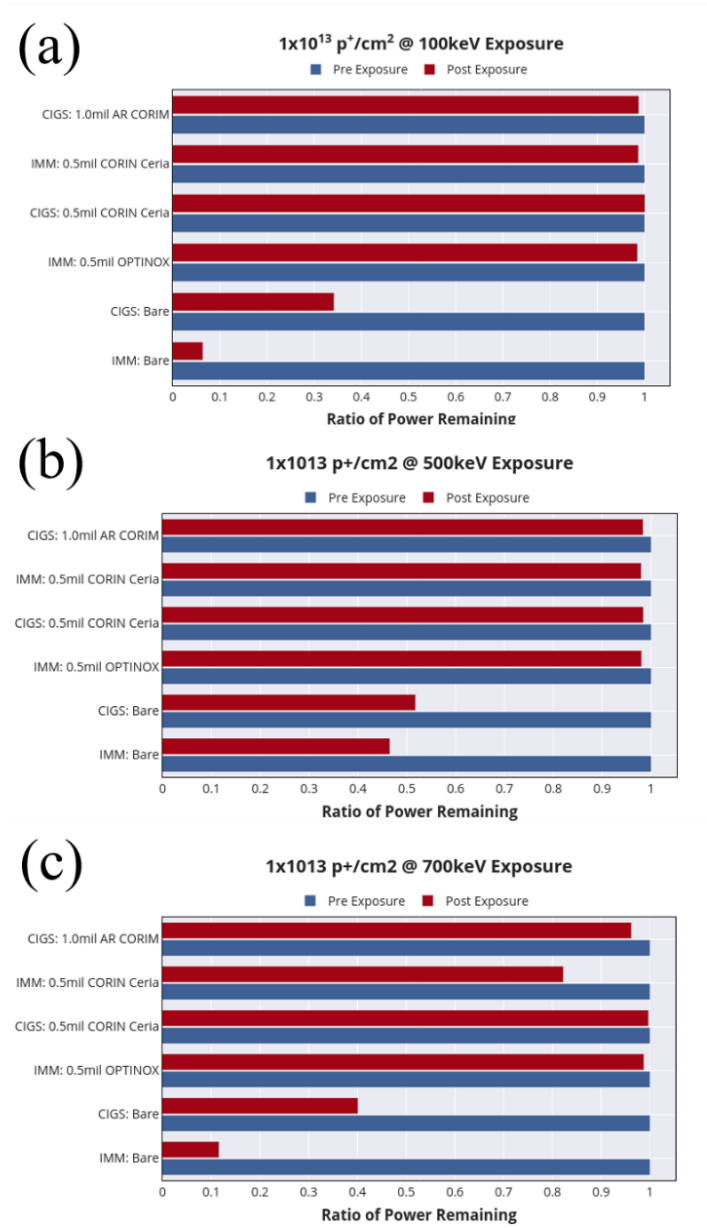

Fig. 16 Power retention of LISA-T cell assemblies after proton energy step up at 1E13p$^+$/cm^2 (a) 100keV, (b) 200keV, and (c) 500keV.

On orbit, radiation damaged cells will heat up during the hot (sunlight) side of the orbit. The literature shows that radiation induced damage in some thin-films may anneal out at relatively lower temperatures (<100 °C), which may be seen on during the LISA-T target missions. To begin to understand these potential annealing effects, 2x IMM and 2x CIGS cells – which had been exposed to 5x10^{15} e$^-$/cm^2 1MeV electron – were heated in a vacuum oven to ~100°C for 1 hour and, subsequently, to ~170 °C for 8 hours (**Fig. 17**). The former is a realistic on-orbit environment that may be encountered, while the latter is an 'extremes experiment' to help set bounds and add to overall understanding. Both

CIGS and IMM saw a modest improvement after 100 °C 1hour anneal, 1.4% and 2.4% respectively. Remember, the CIGS cells saw essentially no degradation through 1 MeV e- at this fluence. It seems likely this gain was realized from another mechanism – which will be seen again in the subsequent section on thermal cycling. The IMM assemblies had lost 30% power generation capability through 1 MeV $4x10^{15}$ e^-/cm^2, gaining only a modest 2.4% recovery through the anneal. It is possible that the multiple hot cycles seen in a LEO orbit may further anneal out damage. Interestingly, the IMMs had a further increase at the longer, hotter anneal (4.3% total), while the CIGS saw a net loss (-2.9%). Seemingly, the CIGS were pushed past their upper temperature limit and began to degrade. Though not reported herein, this high temperature degradation of the CIGS assemblies has also been seen in high temperature, long duration operation experiments – with degradation being attributed to the formation of new and/or exaggeration of pre-existing material shunts.

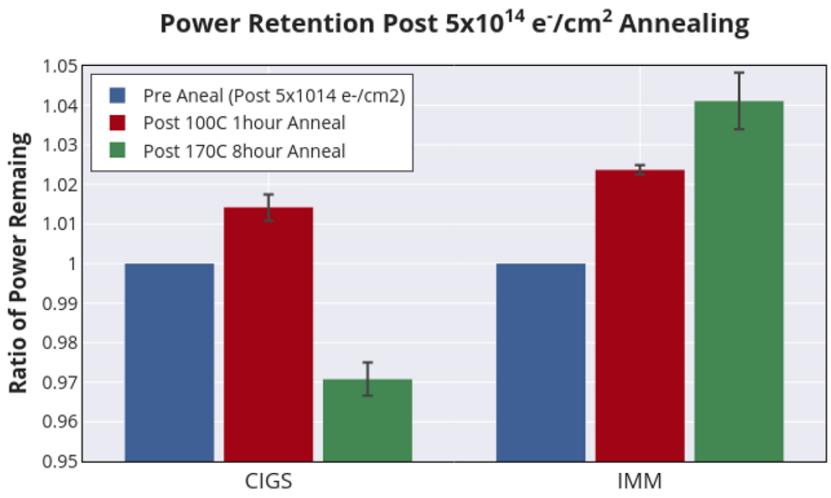

Fig. 17 Power remaining after 5E14e^-/cm^2 @ 1MeV electron radiation annealing experiment

Thermal Cycling

Samples were thermally cycled for 750 cycles from +117 °C to -68 °C (target) and for 750 cycles from +7 °C to -118 °C (target). All temperatures were based on extremes for a representative LISA-T mission with transition rates and dwell times similar to the mission profile. Samples were held under vacuum, raised into a liquid nitrogen cooled cold box during the cold cycle, and subsequently lowered into an infrared lamp array with a stainless-steel radiator plate to increase thermal uniformity for the hot side. 16 measurement thermocouples monitored the experiment.

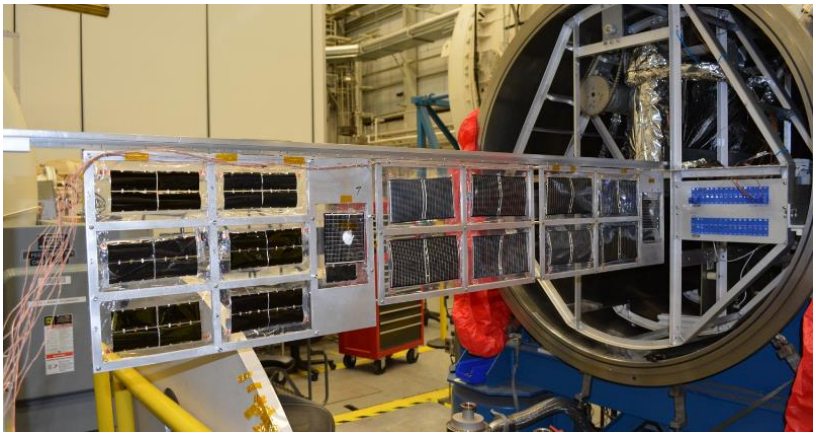

Fig. 18 LISA-T cell assemblies under rapid thermal cycling.

Fig. 18 shows both CIGS and IMM cell assemblies under thermal cycling. **Fig.** 19 highlights the rapid thermal cycling results. The sample temperature data highlights the thermal couple spreads, rise and fall times, and dwell times. Both the IMM and CIGS assemblies performed well. The IMM assemblies, both with and without Elgiloy® and SMA components bonded, retained ~100% power through the three runs. The CIGS assemblies all showed measurable *improvement* through the experiment; similar to the annealing results discussed above. The CP1 bonded CIGS-CORIN®XLS assemblies – with and without backside structural components – improved ~10.7% and 11.1% respectively. Interestingly, several electrical interconnects between cells and cell to bus bar on the bare assemblies – those without a topside coating – broke under the thermal load. None of the interconnects on coated cells were damaged. This supports interconnect pull tests, which showed a significant improvement of connection yield after the coatings were applied (**Fig. 20**). A proprietary anti-reflective (AR) coating, fabricated from CORIN®XLS, was also included on two CIGS assemblies. In both cases, the coating peeled from the cell during run #1 and further peeled during runs #2 and #3. Straight cell coatings are liquid processed, while the AR coatings are cast separately and then bonded to the cell surface without adhesive. Under thermal stress, resin used in the adhesiveless process released, allowing the coating to pull up from the cell. No delamination or degradation was noted for the backside elements.

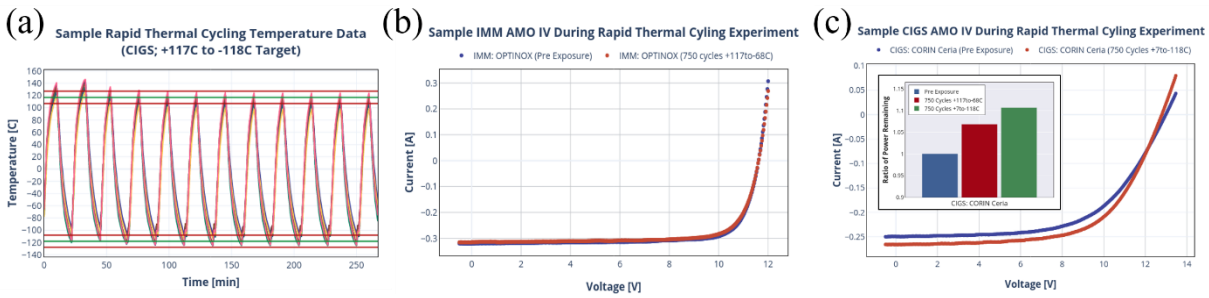

Fig. 19 Rapid thermal cycling results: (a) sample temperature data, (b) sample CP1 bonded IMM-Optinox®SR data, and (c) sample CP1 bonded CIGS-CORIN®XLS data. Insert shows CIGS assembly improvements.

Several samples were also thermally shocked. This is very similar to the thermal cycling done above; however, exposure is done at atmosphere and without control of ramp rates and dwell times. Essentially very rapid switches from hot to cold and vice versa to strain coefficient of thermal expansion mismatches and brings about potential bonding, delamination, etc. failure modes. Samples were shocked through ~210°C of temperature differential (-60 through +150°C) for approximately 35 cycles.

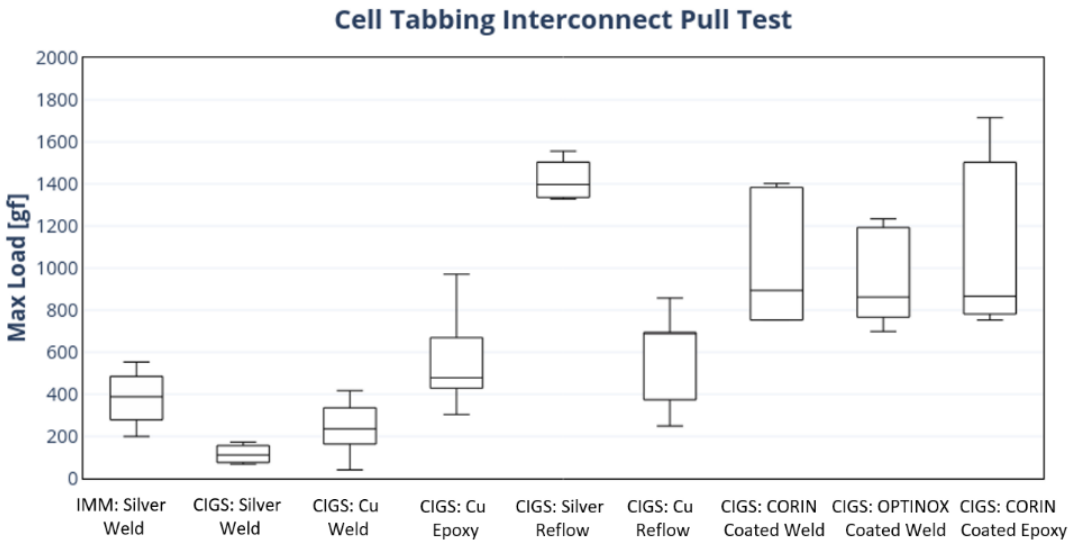

Fig. 20 Tabbing interconnect pull test on LISA-T cell assemblies.

Fig. 21 shows a CIGS sub-coupon + boom elements under test. Two straight cast CORIN®XLS and two AR CORIN®XLS were tested. Segments of the mast boom, spar boom, SMA wire, and copper tracing were included on the back side. The straight coated assemblies performed well. No delamination was noted, and one cell's power output again improved throughout the test. In contrast, both AR cells continually degraded. The AR coatings again began to delaminate from the cell and, further, the cell began to delaminate from the substrate due to strong pull and stiffening of the delaminating coating. Again, no delamination or degradation was noted for the backside elements. IMM cell assemblies were also tested. Delamination of CORIN®XLS was found; Optinox®SR performed well. The bond promoter for the CORIN®XLS process was reformulated and assemblies were successfully cycled.

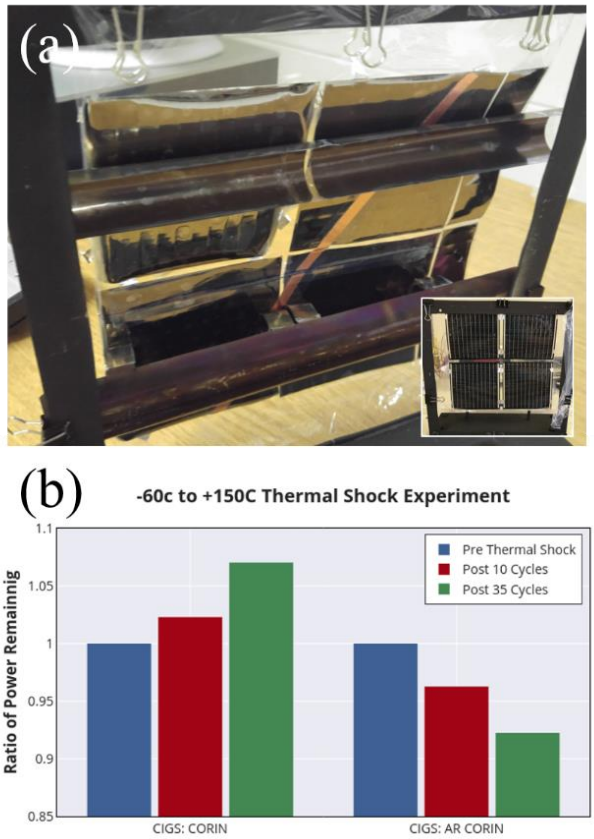

Fig. 21 LISA-T CIGS cell assembly thermal shock (a) under test and (b) power retention data

Ultraviolet Radiation

Subassemblies were exposed to upwards of 2,000 Equivalent Sun Hours (ESH) of Middle and Near Ultraviolet (M-NUV) radiation under high vacuum ($\leq 5 \times 10^{-6}$ torr). Exposure was to wavelengths between 230 and 400 nm at ~1 to 1.6x equivalent suns (calibrated with a spectral radiometer and monitored *in-situ via* a photo diode). Two different setups, denoted Setup A and Setup B, were used. Both coated and uncoated CIGS and IMM cells were exposed. **Fig.** 22 shows sample M-NUV exposure plates before and after testing. A film of Colorless Polyimide 1 (CP1™), known to yellow rapidly under M-NUV, was included behind the cells to track uniformity of the exposure.

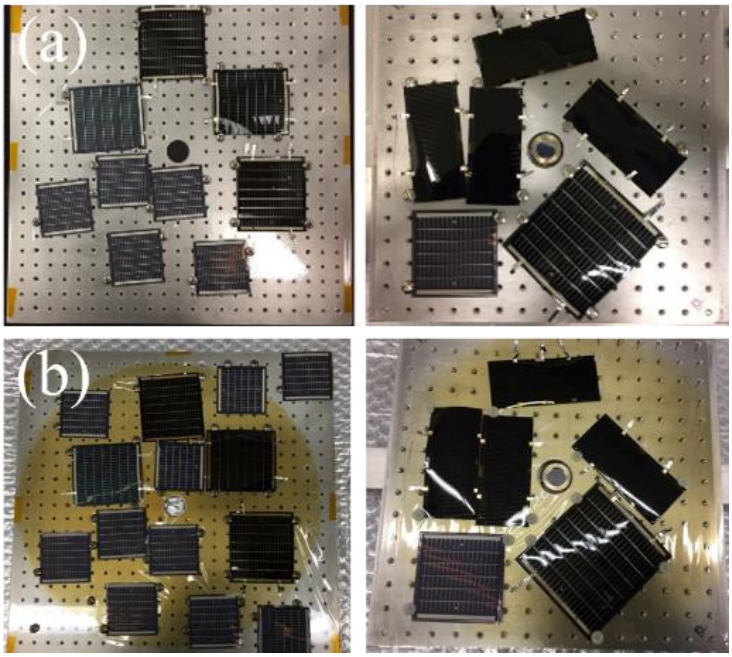

Fig. 22 LISA-T M-NUV testing (a) before and (b) after exposure.

Fig. 23 shows power remaining versus ESH for the M-NUV exposed assemblies. The bare IMM assembly was very tolerant of UV, retaining >98.5% power after 2,000 ESH. The bare CIGS modules, however, rapidly degraded. After ~2,000 ESH, the best cells retained ~65-70% power. It was noticed that after some time, power retention on some bare CIGS cells broke the logarithmic fit and dropped <50% power. This cutoff was seen in three cells and occurred at different ESH – 1277 hours, 1613 hours, and 2555 hours. The CIGS degradation was mostly noted in open circuit voltage. On CIGS assemblies, CORIN®XLS coatings with and without ceria gave significant improvement over the bare assemblies. The CORIN®XLS devices retained 86.5% power after 1,578ESH (85.5% projected for 2,000 ESH). The addition of ceria brought power retention to >90.0% after 2,000ESH; likely stemming from the ability of ceria to subside the formation of color centers.[22] In both cases, degradation was seen in both voltage and current – a combination of the voltage degradation seen in the bare CIGS modules alongside a yellowing of the polyimide coating. CORIN®XLS has a 50% UV cut-off at ~390nm and the top film is absorbing a significant amount of the M-NUV energy. However, though the film yellows, it does so at a slower rate than the UV degradation of the bare cell, yielding a net gain for the coated CIGS cells. In the case of the IMM assemblies, the outcome was opposite. Power retention with CORIN®XLS coatings was significantly lessened when compared to the bare modules; these cells retained 80.8% power after 2,000 ESH while the CORIN®XLS with ceria cells retained 90.45% after 1,115 ESH

(83.8% projected at 2,000 ESH). In both cases, degradation was in the generated current – stemming from the yellowing of the polyimide. This give a net loss compare with the M-NUV stable bare cells.

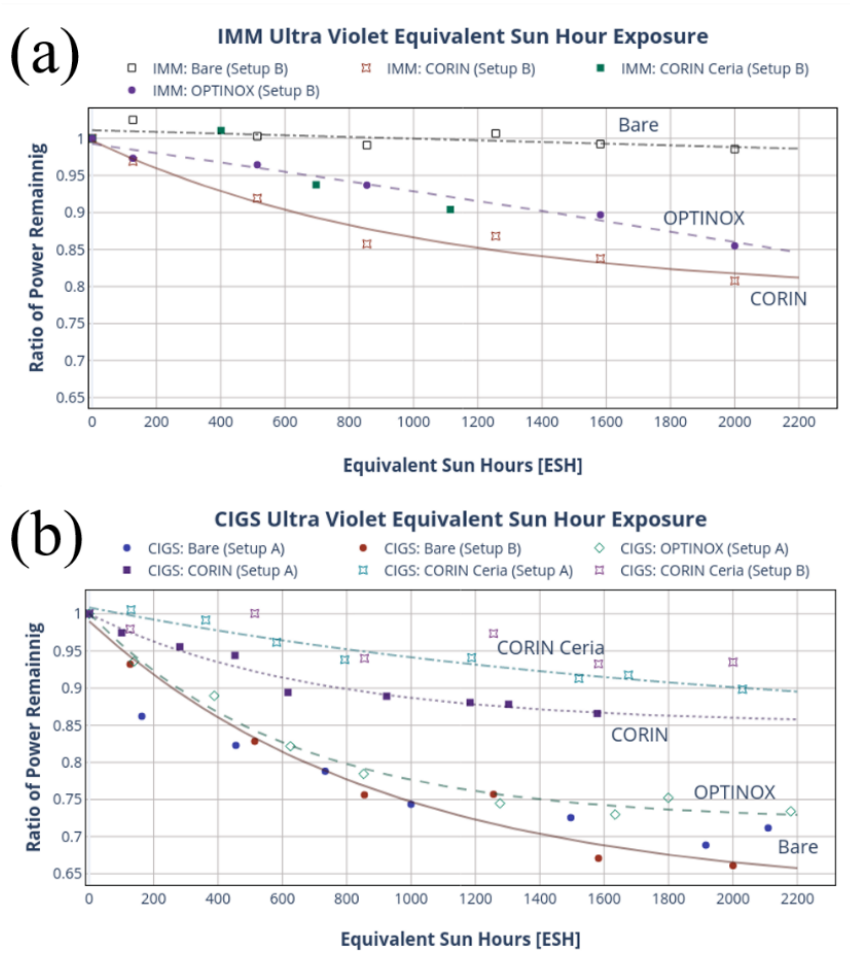

Fig. 23 LISA-T M-NUV testing power reaming versus exposure ESH (a) IMM based assemblies and (b) CIGS base assemblies.

With Optinox®SR coatings, the CIGS assemblies lagged behind the CORIN®XLS coatings, retaining just 73.4% power after 2,180 ESH. The IMM performed modestly better, retaining 85.5% after 2,000 ESH. Degradation of the IMM assemblies was again solely due to loss in current – caused by yellowing of the Optinox®SR coating. The data indicates that Optinox®SR is yellowing more slowly that the CORIN®XLS; a result of the lower UV cut-off of Optinox®SR (50% at 288 nm). Similarly, in the case of the CIGS assemblies, because more M-NUV was reaching the cells, a quicker degradation – of the cell itself – was seen with the Optinox®SR coating. This initial data indicates a CORIN®XLS-ceria approach for CIGS assemblies with either CORIN®XLS-ceria or Optinox®SR for IMM. Future, longer duration applications should explore approaches incorporating UV reflectors onto these assemblies.

Other potential coatings can also be explored depending on the specific radiation environment and expected UV lifetime.

Estimated Survivability

The above testing data was compiled and projected to give an estimate on the survivability of the LISA-T array at 400 km for ~6 months. Note that the projected ballistic coefficient of a representative LISA-T power spacecraft would likely cause the craft to deorbit from 400 km in weeks as opposed to months. However, 400 km serves as an advantageous orbit to begin building survivability models as data can be correlated to International Space Station platforms and subsequently extended out to higher orbits. Survivability is estimated from the total from environmental exposure; operational temperature is not included. Average, best, and worst-case data is shown (**Table 6**). Often, the worst case scenario is far too conservative, but is included for reference. It is likely that as manufacturing matures, survivability will fall between the average and best cases. Some values are calculated and estimated by similarity from other cell assemblies.

Table 6 Summary of initial survivability estimates for top candidate 3rd generation LISA-T solar cell assemblies.

CIGS: CORIN Ceria	**Best**	**Worst**	**Average**
Humidity Exposure	99.1%	90.6%	97.2%
Electrons Exposure	100%	99.0%	99.5%
Protons Exposure	100%	98.0%	99.0%
M-NUV Exposure	93.5%	88.9%	91.2%
Atomic Oxygen Exposure	100%	100%	100%
Thermal Cycling	109%	100%	105%
6 month ISS Power Retention	101%	78.1%	91.7%
IMM: OPTINOX	**Best**	**Worst**	**Average**
Humidity Exposure	100%	96.2%	98.4%
Electrons Exposure	94.0%	92.4%	93.2%
Protons Exposure	100%	99.0%	99.5%
M-NUV Exposure	88.2%	88.2%	88.2%
Atomic Oxygen Exposure	104%	97.6%	101%

Thermal Cycling	99.0%	97.8%	98.4%
6 month ISS Power Retention	85.4%	74.1%	80.0%

The bare CIGS data clearly indicates environmental protection is needed. Only ~45-60% of power would be retained after the 6 month mission. The array would need to be 2x larger to accommodate. Early indications, however, show CIGS CORIN®XLS with ceria gives significant protection to the cell. 87- 92% of power would be retained. In the case of the IMM PV, Optinox®SR is the current top performer, retaining 84-87%. Interestingly, the bare cells weren't much lower at 80-85%. However, the coated cell will filter all particulate radiation below ~1 MeV with very little damage at moderate fluences. In contrast, the bare cell will degrade moderately. Though 50 keV proton testing is include in the table, the slew of other energies that will be present in space may degrade the bare cell further. The coated cell is likely the best option.

On-going work: Advanced testing and a TRL7 flight demo

On November 15, 2018 35x LISA-T samples, including solar cell stack ups, bare materials, and an antenna sample were launched to the International Space Station (ISS) as a part of the MISSE mission #10. The samples are being exposed on-orbit to the zenith side of ISS for one year, which begun on January 15th, 2019, and will be returned to Earth for testing in early 2020. These results will be used to refine the survivability models being built with the ground test data above and help set the focus of future testing. Coupled with this advanced MISSE testing is advanced testing of the mechanical systems. On November 20th, 2019 the LISA-T team rode 60 parabolas on Zero-G's 'G-Force One', systematically deploying LISA-T in the simulated microgravity environment. The weightlessness experienced in each parabola allowed for full freedom of motion testing of the mechanical systems as well as a detailed study of the deployment kinematics. The MISSE-10 electrical and materials results as well as the mechanical parabolic outcomes are currently being analyzed.

The LISA-T program is currently developing an in-space, TRL7 technology demonstration mission. The mission has a target launch date in late 2021 and will demonstrate the deployment, power generation capability, and antenna operation of the array. This mission will run for six months or longer to monitor survivability and degradation. An overview of the mission design, objectives, and requirements will be released following this manuscript.

Conclusions

Herein, third generation advancements and TRL6 testing of the Lightweight Integrated Solar Array and anTenna (LISA-T) have been presented. Building on early generation one and two prototypes, generation three closed the design with significant advancement of the mechanical and electrical systems. Two configurations, namely the planar and omnidirectional, have been demonstrated. Both were designed, fabricated, and deployed on a benchtop gravity offload rig. The system components, including deployment mechanisms, actuators, material sets, solar cell assemblies, etc., were successfully demonstrated in relevant environments targeting small spacecraft operation in LEO. Pre-qualification data on cell assembly lifetime in the relevant environment was also collected. This data forms the basis of survivability modeling and will be correlated to advanced, on-orbit testing currently being conducted on ISS's MISSE-FF platform. LISA-T continues to progress – advanced deployment testing in simulated microgravity as well as a 6U CubeSat technology demonstration mission are on-going. Ultimately, LISA-T will enable the next generation of high power, highly capable small spacecraft.

Funding Sources

This work was funded by NASA's Space Mission Technology Directorate (STMD) Small Spacecraft Technology Program.

References

1. Simburger, E. J., Matsumoto, J. H., Giants, T. W., Garcia III, A., Liu, S., Rawal, S. P., Perry, A. R., Marshall, C. H., Lin, J. K., and Scarborough, S. E. "Thin-film technology development for the PowerSphere," *Materials Science and Engineering: B* Vol. 116, No. 3, 2005, pp. 265-272.

2. Stribling, R. "Boeing high power thin film solar array," *4th International Energy Conversion Engineering Conference and Exhibit (IECEC)*. 2006, p. 4013.
3. Zuckermandel, J., Enger, S., and Gupta, N. "Design, build, and testing of TacSat thin film solar arrays," *4th International Energy Conversion Engineering Conference and Exhibit (IECEC)*. 2006, p. 4198.
4. Zuckermandel, J. W., Enger, S., Gupta, N., and Summers, J. "Modular, thin film solar arrays for operationally responsive spacecraft," *2007 IEEE Aerospace Conference*. IEEE, 2007, pp. 1-6.
5. Breen, M. L., Streett, A., Cokin, D., Stribling, R., Mason, A., and Sutton, S. "IBIS (Integrated Blanket/Interconnect System), Boeing's solution for implementing IMM (Inverted Metamorphic) solar cells on a light-weight flexible solar panel," *2010 35th IEEE Photovoltaic Specialists Conference*. IEEE, 2010, pp. 000723-000724.
6. Lichodziejewski, D., Veal, G., Helms, R., Freeland, R., and Kruer, M. "Inflatable rigidizable solar array for small satellites," *44th AIAA/ASME/ASCE/AHS/ASC Structures, Structural Dynamics, and Materials Conference*. 2003, p. 1898.
7. Reed, K., and Willenberg, H. J. "Early commercial demonstration of space solar power using ultra-lightweight arrays," *Acta Astronautica* Vol. 65, No. 9-10, 2009, pp. 1250-1260.

8. Carr, J. A., Boyd, D., Martinez, A., SanSoucie, M., Johnson, L., Laue, G., Farmer, B., Smith, J. C., Robertson, B., and Johnson, M. "The Lightweight Integrated Solar Array and Transceiver (LISA-T): second generation advancements and the future of SmallSat power generation," 2016.

9. Lockett, T. R., Martinez, A., Boyd, D., SanSoucie, M., Farmer, B., Schneider, T., Laue, G., Fabisinski, L., Johnson, L., and Carr, J. A. "Advancements of the lightweight integrated solar array and transceiver (LISA-T) small spacecraft system," *2015 IEEE 42nd Photovoltaic Specialist Conference (PVSC)*. IEEE, 2015, pp. 1-6.
10. Johnson, L., Carr, J. A., and Boyd, D. "The Lightweight Integrated Solar Array and anTenna (LISA-T) Big Power for Small Spacecraft," 2017.

11. Murphey, T. W., Sanford, G. E., and Jeon, S. "Deployable space boom using bi-stable tape spring mechanism." Patent, 2014.
12. LLC., N. H. 2020. "CP1 Datasheet," http://www.nexolvematerials.com/low-cure-polyimides/cp1-polyimide
13. Finckenor, M., Rodman, L., and Farmer, B. "Analysis of Fluorinated Polyimides Flown on the Materials International Space Station Experiment," 2015.

14. Johnson, L., Young, R., Montgomery, E., and Alhorn, D. "Status of solar sail technology within NASA," *Advances in Space Research* Vol. 48, No. 11, 2011, pp. 1687-1694.

15. Johnson, L., Castillo-Rogez, J., and Dervan, J. "Near Earth Asteroid Scout: NASA's Solar Sail Mission to a NEA," 2017.

16. LLC, N. H. 2020. "CORIN Datasheet," http://www.nexolvematerials.com/low-cure-polyimides/corin-xls-polyimide
17. Wilt, D., Howard, A., Snyder, N., Sahlstrom, T., Heersema, N. A., Nathan, L., Ohshima, T., Sato, S.-i., and Imaizumi, M. "PseudoMorphic Glass to enable high efficiency space photovoltaic devices," *2011 37th IEEE Photovoltaic Specialists Conference*. IEEE, 2011, pp. 001949-001954.
18. Armbruster, M., Wilt, D. M., Cooper, R. J., and Hoffmann, R. C. "Optical and electrical properties of pseudomorphic glass," *2016 IEEE 43rd Photovoltaic Specialists Conference (PVSC)*. IEEE, 2016, pp. 2554-2557.
19. Wilt, D., Snyder, N., Jenkins, P., and Gray, A. "Novel flexible solar cell coverglass for space photovoltaic devices," *2013 IEEE 39th Photovoltaic Specialists Conference (PVSC)*. IEEE, 2013, pp. 2835-2839.
20. Bodeau, M. "Current and voltage thresholds for sustained arcs in power systems," *IEEE Transactions on Plasma Science* Vol. 40, No. 2, 2011, pp. 192-200.

21. LLC, N. H. 2020. "OPTINOX Datasheet," http://www.nexolvematerials.com/specialty-materials-and-films/optinox
22. Josephs, R. *Solar cell array design handbook*: NASA, 1976.
23. Haynes, G. A. *Effect of radiation on cerium-doped solar-cell cover glass*: National Aeronautics and Space Administration, 1970.
24. Granata, J., Sahlstrom, T., Hausgen, P., Messenger, S., Walters, R., Lorentzen, J., Liu, S., and Helizon, R. "Thin-film photovoltaic proton and electron radiation testing for a meo orbit," *2006 IEEE 4th World Conference on Photovoltaic Energy Conference*. Vol. 2, IEEE, 2006, pp. 1773-1776.
25. Imaizumi, M., Matsuda, S., Kawakita, S., Sumita, T., Takamoto, T., Ohshima, T., and Yamaguchi, M. "Activity and current status of R&D on space solar cells in Japan," *Progress in Photovoltaics: Research and Applications* Vol. 13, No. 6, 2005, pp. 529-543.